COMMUNICATION

Check for updates

Efficient growth and characterization of one-dimensional transition metal tellurides inside carbon nanotubes†

Naoyuki Kanda,[a,b] Yusuke Nakanishi, [ID]*[a] Dan Liu, [ID][c,d] Zheng Liu, [ID][e]
Tsukasa Inoue,[b] Yasumitsu Miyata, [ID][a] David Tománek [ID][c] and Hisanori Shinohara[b]

Atomically thin one-dimensional (1D) van der Waals wires of transition metal monochalocogenides (TMMs) have been anticipated as promising building blocks for integrated nanoelectronics. While reliable production of TMM nanowires has eluded scientists over the past few decades, we finally demonstrated a bottom-up fabrication of MoTe nanowires inside carbon nanotubes (CNTs). Still, the current synthesis method is based on vacuum annealing of reactive $MoTe_2$, and limits access to a variety of TMMs. Here we report an expanded framework for high-yield synthesis of the 1D tellurides including WTe, an previously unknown family of TMMs. Experimental and theoretical analyses revealed that the choice of suitable metal oxides as a precursor provides a useful yield for their characterization. These TMM nanowires exhibit a significant optical absorption in the visible-light region. More important, electronic properties of CNTs can be tuned by encapsulating different TMM nanowires.

Nanocarbon materials – nanoscale substances comprising carbon – have played a crucial role in modern materials science.[1–3] As the nanocarbon research matures, significant efforts have been directed towards creating 'post-nanocarbon' materials. Transition metal chalcogenides have been regarded as the promising candidates for novel low-dimensional materials owing to their versatile chemistry and physics. Over the last decade, mono- or few layers of transition metal *di*chalcogenides have been widely recognized as the ideal platform to investigate 2D physics.[4] On the other hand, their 1D counterparts, which exist in a variety of morphologies including nanoribbons,[5] nanotubes,[6] and nanowires,[7,8] could exhibit properties that can be differentiated from the 2D sheets as well as 1D nanocarbons. For instance, single units of transition metal monochalcogenides (TMMs) – in which atomically thin wires are attracted with each other *via* van der Waals interaction – are 1D metallic wires,[8–10] and thus can serve as ultrathin channels for a 2D integrated circuit. We wish to emphasize that unlike in an infinite 2D sheet, electronic states in NWs are quantized due to their finite width. This fact has been explored extensively in finite-width graphene nanoribbons (GNRs) with a fundamentally different conductance from an infinite graphene monolayer.[11] Similar effects are expected in the systems we study. Furthermore, isolated wires are believed to exhibit torsional motion not seen in the bulk, and thereby change their bandgap depending on their torsional angle,[12] allowing potential applications in electro-mechanical switching devices. Despite the growing interest, only a few kinds of isolated TMM nanowires (NWs) are currently available.[13,14] In particular, the isolation of environmentally unstable tellurides with chemical precision remains a significant challenge. In theory, isolated MoTeNWs could exhibit semiconducting properties that opposite the metallic sulfides and selenides, although their salient properties have never been fully verified by experiments.[15,16]

One promising way to produce the 1D tellurides is by using a template reaction *via* carbon nanotubes (CNTs), in which the assembly of the NWs proceeds in one direction.[17] Thermally and chemically robust CNTs have increasingly been used to produce unstable 1D materials such as atomic wires,[18,19] carbyne,[20,21] diamond nanowires,[22,23] GNRs,[24,25] and molecular arrays.[26,27] Besides acting as a template, CNTs also provide a permanent protection for the exposed edges of NWs from the ambient. Perfect CNTs are chemically as inert as defect-free graphene and cannot be destroyed or removed easily. On the other hand, similar to graphene, carbon nanotubes are rather unreactive. Indeed, we have recently demonstrated the successful growth of MoTeNWs inside CNTs by a

*[a]Department of Physics, Tokyo Metropolitan University, Tokyo 192-0397, Japan.
E-mail: naka24ysk@gmail.com*
[b]Department of Chemistry, Nagoya University, Nagoya 464-8602, Japan
[c]Department of Physics and Astronomy, Michigan State University, East Lansing, Michigan 48824, USA
[d]Theoretical Division, Physics and Chemistry of Materials, Los Alamos National Laboratory, Los Alamos, New Mexico 87545, USA
[e]National Institute of Advanced Industrial Science and Technology, Nagoya 463-8560, Japan

†Electronic supplementary information (ESI) available: Materials, experimental and theoretical techniques, synthesis conditions, chemical and spectroscopic analysis. See DOI: 10.1039/d0nr03129a

vacuum annealing of bulk MoTe$_2$.[28] We found that CNTs do not form covalent bonds to the enclosed NWs and thus should not modify their properties. Atomic-level transmission electron microscopy revealed that MoTeNWs show discontinuous torsion, significantly distinct from continuous twisting of MoSNWs.[29] These unique mechanical properties suggest that MoTeNWs and the related 1D tellurides are distinguishable from other TMMs. In order to further explore their properties, a method for their high-yield growth is needed to be developed. Here we demonstrate efficient production of MoTeNWs inside CNTs and its expansion to WTeNWs, an previously unknown member of the TMM family. Through experimental and theoretical studies, we found that the production yields are highly enhanced by choosing suitable metal oxides as a precursor. Furthermore, their high-yield growth enabled us to study their electronic and optical properties. Our CNT-templated growth of MoTe- and WTeNWs will usher in further experiments to shed light on their unexplored properties and potential applications.

A schematic image of the present strategy for the growth of MoTeNWs is shown in Fig. 1a. We chose MoO$_2$ as precursor in this work. We have previously noted the possibility that molybdenum oxides act as intermediates in the reaction that uses MoTe$_2$ as a precursor. Early literature demonstrated that vacuum annealing of MoTe$_2$ results in the formation of non-volatile Mo solid with Te vapors,[30] suggesting that other chemical species serve as the direct source of Mo instead of bulk MoTe$_2$. High-resolution X-ray photoelectron spectroscopy (XPS) revealed that precursor MoTe$_2$ contains several molybdenum oxides including highly volatile MoO$_2$.[28] Thus, we hypothesized that MoO$_2$ is the direct precursor to MoTeNWs.

Fig. 1b displays a representative high-angle annular dark-field scanning transmission electron microscopy (HAADF-STEM) image of the as-produced samples. The atomic structure of the present NWs is similar to the products from MoTe$_2$, which have a quasi-1D structure consisting with Mo$_3$Te$_3$ triangles stacked alternately along the c-axis of CNTs. The positions of XPS peaks are consistent with those of MoTeNWs inside CNTs (Fig. S1a†). Chemical analysis by energy-dispersive X-ray spectroscopy (EDS) also suggests that the NWs are composed of Mo and Te atoms (Fig. S1b†). All the results indicate direct growth of MoTeNWs from a mixture of MoO$_2$ and Te.

Importantly, this reaction utilizing MoO$_2$ as a precursor significantly enhanced the yield of MoTeNWs. Fig. 2a shows Raman spectra of the samples obtained in the optimized conditions from the two different precursors (Fig. S2†). Raman spectrum of MoTeNWs exhibits a characteristic peak located at 251 cm^{-1}, which is assigned to A$_g$ radial breathing mode (RBM) of Mo cores (Fig. 2b).[28] As for the samples from MoO$_2$ with Te, the intensity ratio of the A$_g$ peak to G-band of CNTs is 19.4%, which is approximately 20 times larger than the corresponding value (~1%) from bulk MoTe$_2$ containing the equivalent amount of Mo atoms (Fig. S3†). The enhanced A$_g$ peak of MoTeNWs revealed an improvement for their production yields. The high-yield synthesis of MoTeNWs was further confirmed by HAADF-STEM images (Fig. 2c and d).

In parallel to the experiments, we performed density functional theory (DFT) calculations to investigate the growth
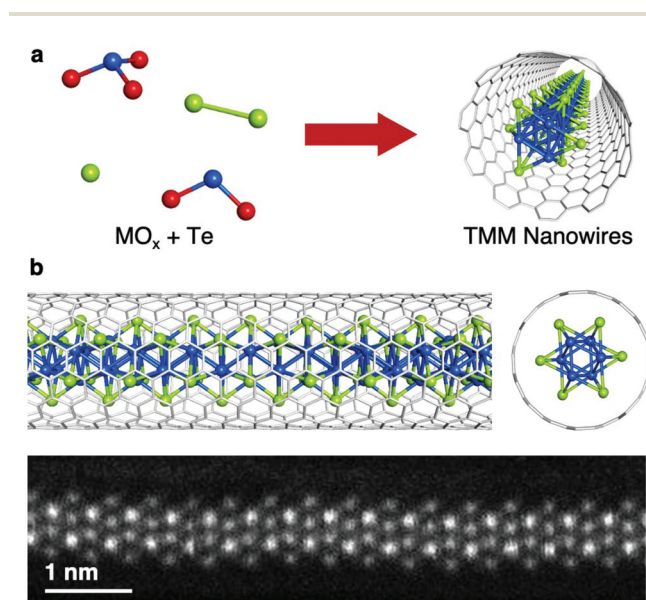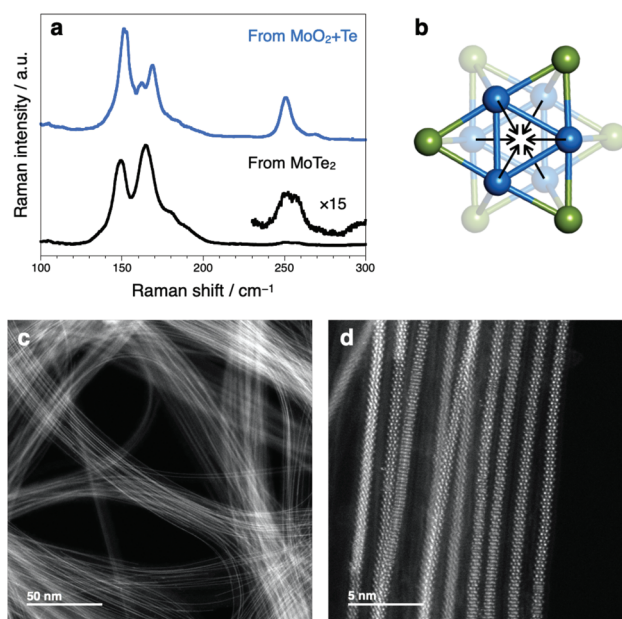

Fig. 1 (a) Schematic of the CNT-templated reaction for the formation of MoTeNWs. (b) A structural model and atomic-resolution HAADF-STEM image of an individual MoTeNW@CNT.

Fig. 2 (a) Raman spectra of MoTeNW@CNTs *via* vacuum annealing of two different precursors (MoTe$_2$ *vs*. MoO$_2$ + Te) at the 633 nm excitation. (b) Schematic of the atomic vibrations for the Raman modes at 251 cm^{-1}. (c and d) HAADF-STEM images of MoTeNW@CNTs.
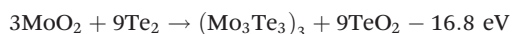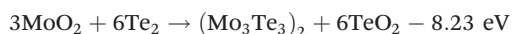
mechanism. The present reaction was rationalized by calculating ΔE for the following reaction:

$$xMoO_2 + yMoO_3 + (x + 1.25y)Te_2 \rightarrow (Mo_3Te_3)_3$$
$$+ (2x + 3y)/2TeO_2 - \Delta E(x + y = 9) \quad (1)$$
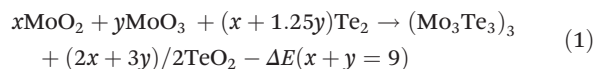
where Mo_3Te_3 represents half the unit cell in an individual MoTeNW. The formation of TeO_2 as a side product was verified by XPS spectra of the residues attached on the surfaces of CNTs.[28] The enthalpy changes for various combinations of (x, y) are summarized in Table 1. Our DFT computation reveals that the reaction in $x \geq 4$ is an exothermic process, and proceeds favorably in terms of thermodynamic energy. In particular, the enthalpy changes for the reaction starting with pure MoO_2 ($x = 9, y = 0$) is the largest (-16.8 eV). This reactivity can be explained by considering that the dissociation of three Mo–O bonds in MoO_3 requires higher energy.[31] These DFT results reveal that MoO_2 plays a key role in the reaction.

Our calculations also indicate that CNTs play a crucial role in the NWs formation. Mo and Te atoms are stabilized on monolayer graphene due to charge transfer between the atoms and the sheet (Fig. S4†), suggesting that the molecules easily get adsorbed on the surfaces of CNTs. Moreover, the electron transfer from MoO_2 to the graphene causes a substantial weakening of the Mo–O bonds (Fig. S5†), and thereby the absorbed MoO_2 can readily react with Te species.

We further calculated ΔE for the sequential extension of Mo_3Te_3 triangles:

$$3MoO_2 + 3Te_2 \rightarrow (Mo_3Te_3)_1 + 3TeO_2 + 1.02 \text{ eV}$$

$$3MoO_2 + 6Te_2 \rightarrow (Mo_3Te_3)_2 + 6TeO_2 - 8.23 \text{ eV}$$

$$3MoO_2 + 9Te_2 \rightarrow (Mo_3Te_3)_3 + 9TeO_2 - 16.8 \text{ eV}$$

A series of reaction enthalpy calculations suggests that the assembled triangles are energetically preferred to isolated ones. This thermodynamic stability favors spontaneous assembly of the NWs. Indeed, the overall length of MoTeNWs reaches a submicron scale, which far exceeds that of typically reported 1D materials inside CNTs.

A possible mechanism for the NWs formation is proposed in Fig. 3. Sublimed MoO_2 and Te_2 molecules are first adsorbed on the outer walls of CNTs. The absorbed molecules can diffuse freely along the surfaces and finally enter the channels due to their stabilization in the inner void.[32,33] As a consequence, the molecules readily react with each other to assemble within CNTs. The self-assembly process occurs repeatedly,
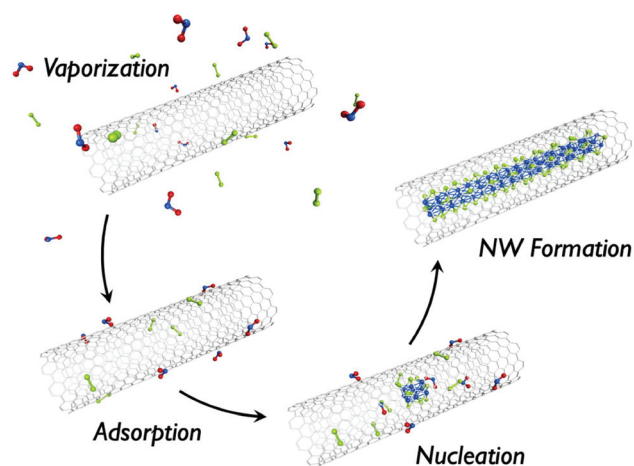

Fig. 3 Possible pathway for growth of MoTeNWs inside CNTs.

resulting in the formation of elongated MoTe NWs. Quasi-1D CNTs serve as a template that prevents the formation of branched structures and bundles by restricting the direction of the chemical reaction.

Based on the present methodology, we further successfully created WTeNWs that have never previously been found in the bulk. A typical HAADF-STEM image of the NWs produced from a mixture of WO_3 and Te is displayed in Fig. 4a. Chemical com-
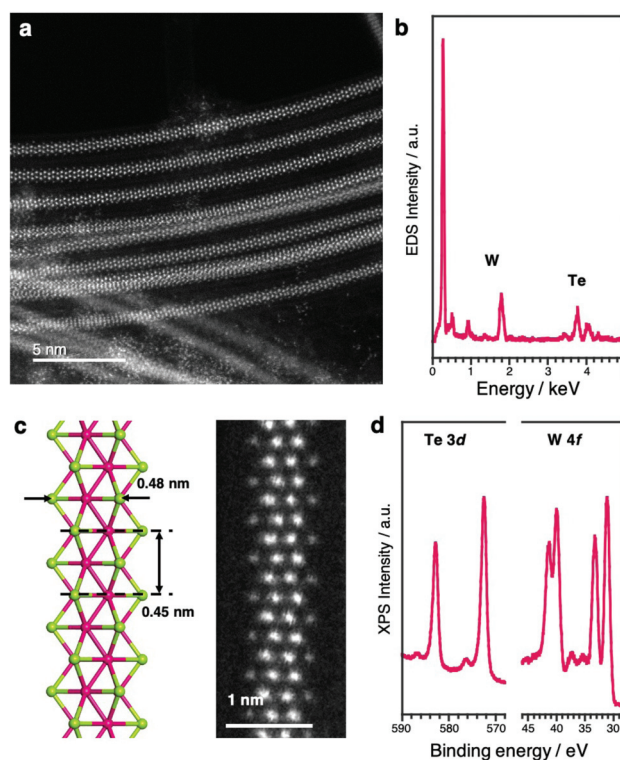

Fig. 4 (a) A typical HAADF-STEM image and (b) EDS analysis of WTeNW@CNTs. (c) A typical HAADF-STEM image and atomic structure of an individual WTeNW. (d) XPS spectra of W 4f and Te 3d core-levels of WTeNWs confined in CNTs.

Table 1 Reaction energy in eqn (1)

x	y	ΔE (eV)
4	5	−0.245
5	4	−3.55
6	3	−6.86
7	2	−10.1
8	1	−13.5
9	0	−16.8

position of the NWs was characterized by the EDS in Fig. 4b, showing that the resultant NWs are composed of W and Te atoms. The axial lattice constant and diameter are measured to be 0.45 and 0.48 nm (Fig. 4c and S6†), which are equivalent to the corresponding values of MoTeNWs and SnSeNWs.[34] The filling yield of WTeNWs is comparable to that of MoTeNWs. In HAADF-STEM images, heavier W atoms (Z = 74) look brighter than Mo atoms (Z = 42) due to the strong electron scattering (Fig. S7†). We found that isolated WTeNWs discontinuously twist similar to MoTeNWs (Fig. S8†), which is significantly distinct from MoS,[29] $NbSe_3$,[35] and $HfTe_3NWs$.[36] Chemical states of WTeNWs confined within CNTs are characterized by XPS. Fig. 4d shows the W 4f and Te 3d core-level XPS spectra, where the peaks at 31.1 and 572.4 eV are assigned to W $4f_{7/2}$ and Te $3d_{5/2}$ of WTeNWs. Compared to WTe_2 layers (31.6 and 572.7 eV), the core-level binding energies for W $4f_{7/2}$ and Te $3d_{5/2}$ show downward shifts by 0.5 and 0.3 eV, respectively. The blue-shifted XPS core-levels are in accord with the peak shift for MoTeNWs.

Efficient growth of these NWs has enabled us to compare their optical and electronic properties. Optical absorption spectra of the products are presented in Fig. 5a. Although the absorption spectra are dominated by the features of template CNTs rather than inner NWs, their spectra commonly show a significant band in the range of 450–600 nm. In order to obtain information on the absorption bands, the electronic structures and density of states (DOS) of isolated MoTe- and WTeNWs were computed by means of DFT calculation. As displayed in Fig. 5b, both of the isolated NWs can be narrow-gap semiconductors in contrast to metallic MoS- and MoSeNWs.[13] Even though DFT is known to underestimate bandgaps, it still can provide useful information about the electronic structure near the Fermi level. Compared to MoTe, the bottom of the conduction band of WTeNWs at the Γ point is lowered, and the band is nearly flat. DFT-based bandgaps between the highest occupied and the lowest unoccupied states of MoTe- and WTeNWs at the Γ point are estimated to be 0.39 and 0.24 eV, respectively. As expected, these values lie well below the absorption bands (2.1–2.8 eV). On the other hand, the energy gaps between the highest occupied and the second lowest unoccupied states at Γ are estimated to be 1.44 eV for MoTeNWs and 1.51 eV for WTeNWs. The DOS diagrams in Fig. 5b suggest a possibility of corresponding inter-band transitions between van Hove singularities. There is little difference in the transition energies between MoTe- and WTeNWs, which also agrees with the experimental results.

Fig. S9† compares Raman spectra of MoTe- and WTeNW@CNTs. As illustrated in Fig. 2a and b, MoTeNWs confined in CNTs exhibit a prominent peak at 251 cm^{-1} originating from RBM mode of Mo cores. In contrast, there is a noticeable peak at 190 cm^{-1} in the spectrum of WTeNW@CNTs. Given that the frequency is inversely proportional to the square root of mass ($f \propto m^{-1/2}$), the peak might be attributed to RBM of W cores. However, the peak may be assigned the shifted RBMs of CNTs due to the interaction with WTeNWs. Additional experiments are needed to figure out the origin of the Raman mode.

Further XPS analyses revealed that the charge transfer occurs between CNTs and the inner NWs. Fig. 5c shows C 1s core-level XPS spectra of MoTeNW@CNTs, WTeNW@CNTs, and pristine CNTs. The C 1s core-level is shifted downward by 0.6 eV after the encapsulation of WTeNWs, which is larger in comparison to MoTeNWs (~0.3 eV). The blue shift of C 1s core-level is considered as a result of electron transfer from CNTs to the NWs.[37,38] Given that the filling yields of these NWs are comparable, WTeNWs exhibit the stronger affinity towards CNTs. The difference in the charge transfer can be understood by considering the difference in electronegativity between Mo and W atoms. The Pauling electronegativity of Mo (χ = 2.16) is almost equivalent to that of Te (χ = 2.1).[39] When Mo atoms are replaced by more electronegative W (χ = 2.36), the electron density in W–Te bonds is further pulled to W atoms. As a consequence, the positively charged Te atoms interact more strongly with inner walls of CNTs, thereby inducing stronger p-type doping of CNTs. This doping should shift the Fermi level and make all filled nanotubes conducting. Indeed, the electrical and thermal transport properties of CNTs are drastically modulated by encapsulated molecules,[40,41] leading to their application in electrical and thermoelectric devices. We expect that confinement of the heavy-metal NWs will induce a significant modulation of transport properties of individual CNTs. A conclusive confirmation of this claim poses, however, a significant challenge. The main reason is that quantum conductance measurements are extremely demanding due to the difficulty to precisely position a nanotube and provide low-resistance ohmic contacts. These issues are currently unsolved and topics of high-priority research.
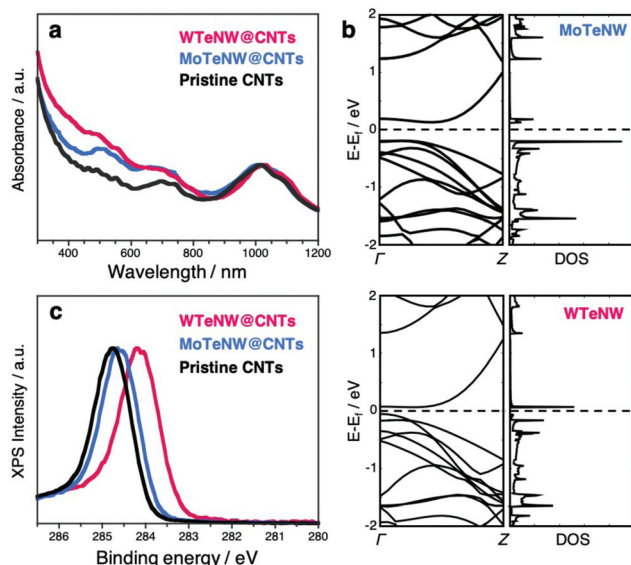

Fig. 5 (a) Optical absorption spectra of MoTe- (blue), WTeNW@CNTs (pink), and pristine CNTs (black). (b) Bandstructures and DOS of isolated MoTe- and WTeNWs. (c) XPS spectra of C 1s core-levels of MoTe- (blue), WTeNW@CNTs (pink), and pristine CNTs (black).

Conclusions

In conclusion, we reported an expanded framework for high-yield synthesis of MoTe- and WTeNWs with chemical precision by utilizing the CNT-templated reaction. Vacuum annealing of suitable metal oxides with Te results in efficient growth of MoTe- and WTeNWs inside CNTs. These 1D products exhibit intense optical absorption peaks in the visible-light range. Also, the inner NWs interact strongly with the outer carbon sheaths, which thereby induce p-type doping of CNTs. Direct measurements of their transport properties are now underway in the present laboratory.

Authors contributions

Y. N. conceived the idea and directed the project. N. K. conducted the sample preparation, spectral characterization, and preliminary TEM observation. Z. L. performed the STEM experiments. D. L. and D. T. performed DFT calculations related to growth and characterization. T. I. and H. S. conducted XPS experiments and analysis. N. K., Y. N., and Y. M. carried out absorption measurements and analyses. Y. N. prepared the manuscript with feedback from the other authors. All authors have given approval to the final version of the manuscript.

Conflicts of interest

There are no conflicts to declare.

Acknowledgements

References

1 H. W. Kroto, J. M. Heath, S. C. O'Brien, R. F. Curl and R. E. Smalley, *Nature*, 1985, **318**, 162–163.
2 S. Iijima, *Nature*, 2002, **354**, 56–58.
3 K. S. Novoselov, A. K. Geim, S. V. Morozov, D. Jiang, Y. Zhang, S. V. Dubonos, I. V. Grigorieva and A. A. Firsov, *Science*, 2004, **306**, 666–669.
4 P. Ajayan, P. Kim and K. Banerjee, *Phys. Today*, 2016, **69**, 38–44.
5 Y. Li, Z. Zhou, S. Zhang and Z. Chen, *J. Am. Chem. Soc.*, 2008, **130**, 16739–16744.
6 P. Chithaiah, S. Ghosh, A. Idelevich, L. Rovinsky, T. Livneh and A. Zak, *ACS Nano*, 2020, **14**, 3004–3016.
7 L. Venkataraman and C. M. Lieber, *Phys. Rev. Lett.*, 1999, **83**, 5334–5337.
8 I. Popov, T. Yang, S. Berber, G. Seifert and D. Tománek, *Phys. Rev. Lett.*, 2007, **99**, 085503–085504.
9 A. Simon, *Angew. Chem., Int. Ed.*, 1988, **27**, 159–183.
10 T. Yang, S. Okano, S. Berber and D. Tománek, *Phys. Rev. Lett.*, 2006, **96**, 125502.
11 M. Y. Han, B. Özyilmaz, Y. Zhang and P. Kim, *Phys. Rev. Lett.*, 2007, **98**, 206805.
12 I. Popov, S. Gemming, S. Okano, N. Ranjan and G. Seifert, *Nano Lett.*, 2008, **8**, 4093–4098.
13 J. Lin, O. Cretu, W. Zhou, K. Suenaga, D. Prasai, K. I. Bolotin, N. T. Cuong, M. Otani, S. Okada, A. R. Lupini, J.-C. Idrobo, D. Caudel, A. Burger, N. J. Ghimire, J. Yan, D. G. Mandrus, S. J. Pennycook and S. T. Pantelides, *Nat. Nanotechnol.*, 2014, **9**, 436–442.
14 J. Lin, Y. Zhang, W. Zhou and S. T. Pantelides, *ACS Nano*, 2016, **10**, 2782–2790.
15 H. Zhu, Q. Wang, C. Zhang, R. Addou, K. Cho, R. M. Wallace and M. J. Kim, *Adv. Mater.*, 2017, **29**, 1606264–1606265.
16 Y. Yu, G. Wang, Y. Tan, N. Wu, X.-A. Zhang and S. Qin, *Nano Lett.*, 2018, **18**, 675–681.
17 J. Sloan and M. Monthioux, in *Carbon Meta-Nanotubes Synthesis, Properties and Applications*, John Wiley & Sons, Ltd, 2011, pp. 225–271.
18 T. Fujimori, A. Morelos-Gómez, Z. Zhu, H. Muramatsu, R. Futamura, K. Urita, M. Terrones, T. Hayashi, M. Endo, S. Y. Hong, Y. C. Choi, D. Tománek and K. Kaneko, *Nat. Commun.*, 2013, **4**, 2162.
19 E. Philp, J. Sloan, A. I. Kirkland, R. R. Meyer, S. Friedrichs, J. L. Hutchison and M. L. H. Green, *Nat. Mater.*, 2003, **2**, 788–791.
20 L. Shi, P. Rohringer, K. Suenaga, Y. Niimi, J. Kotakoski, J. C. Meyer, H. Peterlik, M. Wanko, S. Cahangirov, A. Rubio, Z. J. Lapin, L. Novotny, P. Ayala and T. Pichler, *Nat. Mater.*, 2016, **15**, 634–639.
21 L. Shi, K. Yanagi, K. Cao, U. Kaiser, P. Ayala and T. Pichelar, *ACS Nano*, 2018, **12**, 8477–8484.
22 J. Zhang, Y. Feng, H. Ishiwata, Y. Miyata, R. Kitaura, J. E. P. Dahl, R. M. K. Carlson, H. Shinohara and D. Tománek, *ACS Nano*, 2012, **6**, 8674–8683.
23 J. Zhang, Z. Zhu, Y. Feng, H. Ishiwata, Y. Miyata, R. Kitaura, J. E. P. Dahl, R. M. K. Carlson, N. A. Fokina, P. R. Schreiner, D. Tománek and H. Shinohara, *Angew. Chem., Int. Ed.*, 2013, **52**, 3717–3721.
24 A. V. Talyzin, I. V. Anoshkin, A. V. Krasheninnikov, R. M. Nieminen, A. G. Nasibulin, H. Jiang and E. I. Kauppinen, *Nano Lett.*, 2011, **11**, 4352–4356.
25 A. I. Chernov, P. V. Fedotov, A. V. Talyzin, I. Suarez Lopez, I. V. Anoshkin, A. G. Nasibulin, E. I. Kauppinen and E. D. Obraztsova, *ACS Nano*, 2013, **7**, 6346–6353.

26 G. Pagona, G. Rotas, A. N. Khlobystov, T. W. Chamberlain, K. Porfyrakis and N. Tagmatarchis, *J. Am. Chem. Soc.*, 2008, **130**, 6062–6063.

27 J. H. Warner, A. A. R. Watt, L. Ge, K. Porfyrakis, T. Akachi, H. Okimoto, Y. Ito, A. Ardavan, B. Montanari, J. H. Jefferson, N. M. Harrison, H. Shinohara and G. A. D. Briggs, *Nano Lett.*, 2008, **8**, 1005–1010.

28 M. Nagata, S. Shukla, Y. Nakanishi, Z. Liu, Y.-C. Lin, T. Shiga, Y. Nakamura, T. Koyama, H. Kishida, T. Inoue, N. Kanda, S. Ohno, Y. Sakagawa, K. Suenaga and H. Shinohara, *Nano Lett.*, 2019, **19**, 4845–4851.

29 A. L. Koh, S. Wang, C. Ataca, J. C. Grossman, R. Sinclair and J. H. Warner, *Nano Lett.*, 2016, **16**, 1210–1217.

30 W. A. Brainard, *The Thermal Stability and Friction of the Disulfides, Diselenides, and Ditellurides of Molybdenum and Tungsten in Vacuum (10^{-9} to 10^{-6} Torr)*, NASA, Washington, DC, 1969, pp. 1–22, NASA Technical Note TN D-5141.

31 Even though vacuum annealing of MoO_3 with Te also produces MoTeNWs, the production yield is lower when compared to MoO_2.

32 S. Berber, Y.-K. Kwon and D. Tománek, *Phys. Rev. Lett.*, 2002, **88**, 323–324.

33 Y. Nakanishi, H. Omachi, N. A. Fokina, P. R. Schreiner, R. Kitaura, J. E. P. Dahl, R. M. K. Carlson and H. Shinohara, *Angew. Chem., Int. Ed.*, 2015, **54**, 10802–10806.

34 C. A. Slade, A. M. Sanchez and J. Sloan, *Nano Lett.*, 2019, **19**, 2979–2984.

35 T. Pham, S. Oh, P. Stetz, S. Onishi, C. Kisielowski, M. L. Cohen and A. Zettl, *Science*, 2018, **361**, 263–266.

36 S. Meyer, T. Pham, S. Oh, P. Ercius, C. Kisielowski, M. L. Cohen and A. Zettl, *Phys. Rev. B*, 2019, **100**, 041403.

37 H.-Z. Geng, K. K. Kim, C. Song, N. T. Xuyen, S. M. Kim, K. A. Park, D. S. Lee, K. H. An, Y. S. Lee, Y. Chang, *et al.*, *J. Mater. Chem.*, 2008, **18**, 1261–1266.

38 V. O. Koroteev, L. G. Bulusheva, I. P. Asanov, E. V. Shlyakhova, D. V. Vyalikh and A. V. Okotrub, *J. Phys. Chem. C*, 2011, **115**, 21199–21204.

39 L. Pauling, *J. Am. Chem. Soc.*, 1932, **54**, 3570–3582.

40 T. Kodama, M. Ohnishi, W. Park, T. Shiga, J. Park, T. Shimada, H. Shinohara, J. Shiomi and K. E. Goodson, *Nat. Mater.*, 2017, **16**, 892–897.

41 J. Lee, H. Kim, S. J. Kahng, G. Kim, Y. W. Son, J. Ihm, H. Kato, Z. W. Wang, T. Okazaki, H. Shinohara, *et al.*, *Nature*, 2002, **415**, 1005–1008.